JFM RAPIDS
journals.cambridge.org/rapids

Decaying turbulence beneath surface waves

Gregory L. Wagner[1] † and Navid C. Constantinou[2, 3]

[1]Massachusetts Institute of Technology, Cambridge, MA, USA

[2]University of Melbourne, Parkville, VIC, Australia

[3]ARC Centre of Excellence for the Weather of the 21st Century, Parkville, VIC, Australia

(Received xx; revised xx; accepted xx)

This paper explores decaying turbulence beneath surface waves that is initially isotropic and shear-free. We start by presenting phenomenology revealed by wave-averaged numerical simulations: an accumulation of angular momentum in coherent vortices, suppression of kinetic energy dissipation, and the development of depth-alternating jets. We interpret these features through an analogy with rotating turbulence (Holm 1996), wherein the curl of the Stokes drift, $\nabla \times \boldsymbol{u}^S$, takes on the role of the background vorticity (for example, $(f_0 + \beta y)\,\hat{\boldsymbol{z}}$ on the β-plane). We pursue this thread further by showing that a two-equation model proposed by Bardina *et al.* (1985) for rotating turbulence reproduces the simulated evolution of volume-integrated kinetic energy. This success of the two-equation model — which explicitly parameterizes wave-driven suppression of kinetic energy dissipation — carries implications for modeling turbulent mixing in the ocean surface boundary layer. We conclude with a discussion about a wave-averaged analogue of the Rossby number appearing in the two-equation model, which we term the "pseudovorticity number" after the pseudovorticity $\nabla \times \boldsymbol{u}^S$. The pseudovorticity number is related to the Langmuir number in an integral sense.

1. Introduction

Surface waves enhance near-surface ocean turbulent mixing, especially in summertime and in the tropics where boundary layers are often shallow, sunny, windy, and wavy Sullivan & McWilliams (2010). Turbulence driven by surface wind stress and affected by surface waves is usually called "Langmuir turbulence" McWilliams *et al.* (1997), implying a connection between wave-catalyzed turbulent coherent structures and the structure of a laminar, wave-catalyzed shear instability that Craik & Leibovich (1976) called "Langmuir circulation".

In this paper we investigate decaying turbulence beneath surface waves using numerical simulations of the wave-averaged Navier–Stokes equations (Craik & Leibovich 1976). Decaying turbulence is fundamental (Batchelor 1953) but has seen little attention beneath

† Email address for correspondence: wagner.greg@gmail.com

surface waves. Most work on wave-modified turbulence involves strong ambient shear and also invokes surface forcing by winds and buoyancy fluxes (McWilliams *et al.* 1997; Polton *et al.* 2005; Harcourt & D'Asaro 2008; Van Roekel *et al.* 2012; Large *et al.* 2019; Fan *et al.* 2020). We show that some of the essential phenomology of turbulence beneath surface waves is revealed by focusing on the evolution of unforced, initially-shear-free turbulence.

We interpret the results of these simulations in section 2, leveraging an analogy between wave-averaged and rotating dynamics first proposed by Holm (1996). Like rotation, surface waves *catalyze* an inverse cascade — without exchanging energy with the flow — and cause angular momentum to accumulate in coherent vortices, while suppressing kinetic energy dissipation. We observe the development of alternating jets, as in beta-plane turbulence. In section 3 we further the analogy by adapting a phenomenological model proposed by Bardina *et al.* (1985) for decaying rotating turbulence to the wave-averaged case, showing that the model also describes the decay of volume-averaged kinetic energy beneath surface waves. This model suggests a new way to incorporate wave effects into two-equation models (for example, Harcourt 2015) by explicitly representing the surface-wave-driven suppression of kinetic energy dissipation.

We conclude in section 4 by proposing a new non-dimensional number to characterize the importance of surface waves for the evolution of turbulent flows analogous to the Rossby number. We show how this new number may be related to the Langmuir number for wind-forced cases, while also generalizing to purely convective or decaying situations.

2. Simulations of decaying turbulence beneath surface waves

The incompressible Euler momentum equation in the presence of a background vorticity $\boldsymbol{\Omega}$,

$$\partial_t \boldsymbol{u} + (\boldsymbol{u}\cdot\boldsymbol{\nabla})\,\boldsymbol{u} + \boldsymbol{\Omega}\times\boldsymbol{u} + \boldsymbol{\nabla} p = 0\,, \qquad \text{with} \qquad \boldsymbol{\nabla}\cdot\boldsymbol{u} = 0\,, \tag{2.1}$$

describes both rotating flows and wave-averaged flows beneath steady, horizontally-uniform surface wave fields (Craik & Leibovich 1976; Suzuki & Fox-Kemper 2016; Wagner *et al.* 2021). In the wave-averaged case, $\boldsymbol{u}$ in (2.1) is is the Lagrangian-mean momentum and p is Eulerian-mean kinematic pressure. To use (2.1) for rotating flows we take

$$\boldsymbol{\Omega}_{\text{rotating}} = f\,\hat{\boldsymbol{z}}\,, \tag{2.2}$$

where f is the Coriolis parameter and $\hat{\boldsymbol{z}}$ is the axis of rotation. For wave-averaged flows we take

$$\boldsymbol{\Omega}_{\text{waves}} = -\boldsymbol{\nabla}\times\boldsymbol{u}^{\text{S}} = -\partial_z u^{\text{S}}\,\hat{\boldsymbol{y}}\,, \tag{2.3}$$

where $\boldsymbol{u}^{\text{S}} = u^{\text{S}}(z)\,\hat{\boldsymbol{x}}$ is the Stokes drift of a surface wave field propagating in the $\hat{\boldsymbol{x}}$-direction. In the context of equation 2.1, the main difference between rotating turbulence and turbulence beneath steady surface waves is the spatial structure of $\partial_z u^{\text{S}}$: in shallow water $\partial_z u^{\text{S}} \sim z$ to leading-order, while $\partial_z u^{\text{S}}$ decays exponentially for deep water waves.

2.1. *Coherent structures in rotating and wave-averaged turbulence*

To illustrate the similarity of rotating turbulence and turbulence beneath surface waves we conduct large eddy simulations of equation (2.1) in a unit cube with three choices for $\boldsymbol{\Omega}$,

$$\boldsymbol{\Omega}_{\text{rotating}} = \tfrac{1}{4}\,\hat{\boldsymbol{z}}\,, \qquad \boldsymbol{\Omega}_{\text{waves}} = -\tfrac{1}{2}\,z\,\hat{\boldsymbol{y}}\,, \quad \text{and} \quad \boldsymbol{\Omega}_{\text{isotropic}} = 0\,. \tag{2.4}$$

Above, $\boldsymbol{\Omega}_{\text{waves}}$ is the pseudovorticity associated with a shallow water wave in $z \in [0,1]$ with Stokes drift $\boldsymbol{u}^{\text{S}} \approx \frac{1}{2}\big(1+\frac{1}{2}z^2\big)\,\hat{\boldsymbol{x}}$.

We produce an initial condition for the three simulations by conducting a preliminary simulation initialized with kinetic energy spectrum

$$\tfrac{1}{2}|\hat{\boldsymbol{u}}|^2 \sim |\boldsymbol{K}|^2 \exp\left\{-2\,(|\boldsymbol{K}|/K_i)^2\right\}\,, \tag{2.5}$$

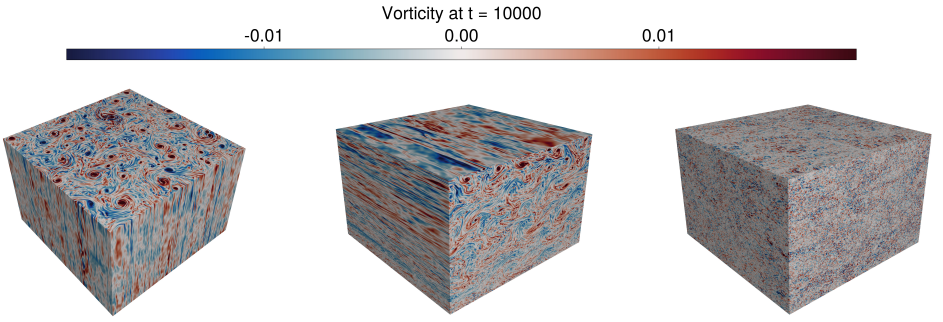

Figure 1: Vorticity in simulations decaying turbulence with 512^3 finite volume cells in a unit cube after 1000 time units. (a) Vertical relative vorticity $\zeta = \hat{\boldsymbol{z}} \cdot (\boldsymbol{\nabla} \times \boldsymbol{u})$ in rotating turbulence with Coriolis parameter $f = 1/4$, (b) Horizontal relative vorticity $\eta = \hat{\boldsymbol{y}} \cdot (\boldsymbol{\nabla} \times \boldsymbol{u})$ in turbulence beneath surface waves with Stokes shear $\partial_z u^{\mathrm{S}} = -z/2$, and (c) η in isotropic turbulence.

where $\hat{\boldsymbol{u}}$ is the Fourier transform of $\boldsymbol{u}$, $\boldsymbol{K}$ is the Fourier wavenumber vector, and $K_i = 32 \times 2\pi$ is the 32^{nd} wavenumber in the domain. The amplitude of the preliminary initial condition is scaled to produce an initial root-mean-square vorticity

$$\sqrt{\int |\boldsymbol{\omega}|^2 \, \mathrm{d}V} \overset{\text{def}}{=} \omega_{\mathrm{rms}}(t = -t_0) = 1000\,, \quad \text{where} \quad \boldsymbol{\omega} \overset{\text{def}}{=} \boldsymbol{\nabla} \times \boldsymbol{u} = \xi \hat{\boldsymbol{x}} + \eta \hat{\boldsymbol{y}} + \zeta \hat{\boldsymbol{z}}\,. \tag{2.6}$$

The initial simulation is run for a duration t_0 until $t = 0$, defined as the time when the mean-square vorticity has decayed to $\omega_{\mathrm{rms}}(t = 0) = 10$. The velocity field is then saved to disk to be used as an initial condition in subsequent runs starting from $t = 0$. The simulations are conducted with Oceananigans (Ramadhan *et al.* 2020; Wagner *et al.* 2025), which discretizes (2.1) with a finite volume method. We use a nominally 9th-order Weighted, Essentially Non-Oscillatory advection scheme (Shu 2020), which dissipates kinetic energy at the grid scale. Scripts that reproduce simulations in this paper are stored on GitHub; see the Data availability statement.

We focus first on the evolution of the relative vorticity $\boldsymbol{\omega}$ defined in equation (2.6). Figure 1 shows vorticity components for the three cases after $t = 1000$ time units: figure 1(a) shows vertical vorticity ζ, while while figures 1(b) and (c) show the horizontal vorticity η. Figure 1(a) and (b) for rotating and wave-affected turbulence, respectively, both exhibit the formation of coherent structures and relatively greater vorticity levels than the unorganized, small amplitude isotropic vorticity in figure 1(c). Figure 2 is similar, except that figure 2(a) shows ζ in rotating turbulence in the xy-plane, while figures 2(b) and (c) show η in the xz plane for wave-averaged and isotropic turbulence, respectively.

2.2. *Zonation and the analogy of wave-averaged turbulence with beta-plane turbulence*

Note that turbulence beneath shallow water waves is homeomorphic to β-plane turbulence Rhines (1975) — with $\boldsymbol{\Omega}_{\beta\text{-plane}} = \beta y \hat{\boldsymbol{z}}$ — modulo on the xz plane instead of on the xy plane. One of the most striking results of this similarity is the propensity for turbulence beneath surface waves to develop "zonal jets" — coherent, alternating jets in the direction of surface wave propagation (and perpendicular to the pseudovorticity direction). This similarity allows us, therefore, to borrow intuition on structure formation in β-plane turbulence (for example, Huang & Robinson (1998); Farrell & Ioannou (2007); Srinivasan & Young (2012);

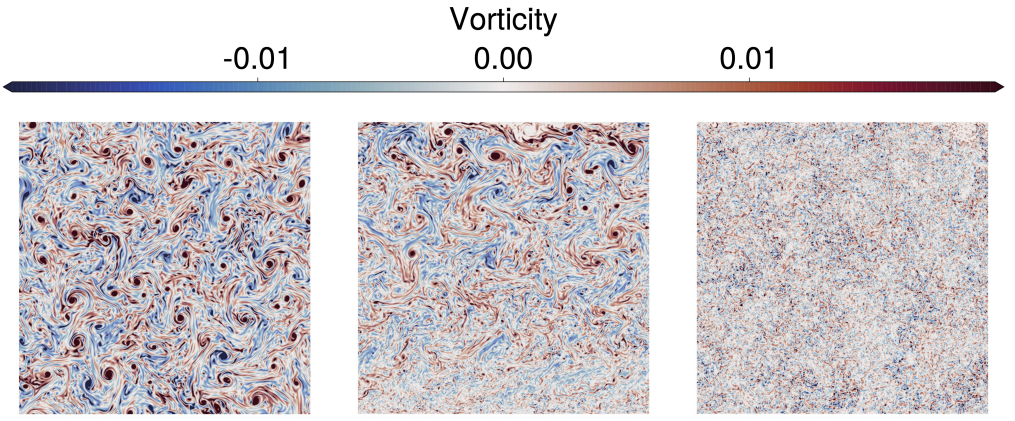

Figure 2: As figure 1 but showing (a) ζ for rotating turbulence in the xy-plane; (b) η for turbulence beneath surface waves in the xz-plane, (c) η for isotropic turbulence in the xz-plane.

Constantinou *et al.* (2014); for an overview see Constantinou (2015); Farrell & Ioannou (2019); Marston & Tobias (2023).)

To illustrate this, we consider two additional cases with pseudovorticity

$$\boldsymbol{\Omega}_{\text{deep}} = \tfrac{1}{4}\mathrm{e}^{8(z-1)}\,\hat{\boldsymbol{y}}\,. \qquad \text{and} \qquad \boldsymbol{\Omega}_{\text{weak}} = \tfrac{1}{8}z\,\hat{\boldsymbol{y}}\,. \tag{2.7}$$

These and subsequent simulations use 384^3 finite volume cells.

Figure 3 shows time-series of the y-momentum v, which plays the role that vertical velocity plays in rotating turbulence, as well as vertical profiles of the horizontally-averaged x-momentum,

$$U(z,t) \overset{\text{def}}{=} \int u\,\mathrm{d}x\,\mathrm{d}y\,, \tag{2.8}$$

The profiles of U on the right side of figure 3 exhibit the development of depth-alternating jets, which to our knowledge has not yet been observed in shear-free wave-modified turbulence. Comparing the slices of v for medium and weak waves reveals how the medium-strong waves induce a strong inverse cascade, more coherent vortices, and fewer small-scale motions than the weak waves.

3. Phenomenological model for the evolution of kinetic energy

We turn to the evolution of the domain-averaged kinetic energy,

$$k(t) \overset{\text{def}}{=} \int \tfrac{1}{2}\left(u^2+v^2+w^2\right)\,\mathrm{d}V\,. \tag{3.1}$$

Figure 4 plots time-series of the normalized kinetic energy $k(t)/k(t=0)$ for the three cases presented in figure 1, as well as three additional cases that use $\boldsymbol{\Omega} = Sz\hat{\boldsymbol{y}}$ with $S = (1/2, 1/8, 1/16)$. Figure 4 illustrates another common feature to rotating turbulence and turbulence beneath surface waves: a suppression of the kinetic energy dissipation rate, such that at long times the kinetic energy levels off.

Inspired by Bardina *et al.* (1985), we model $k(t)$ with the phenomenological two-equation

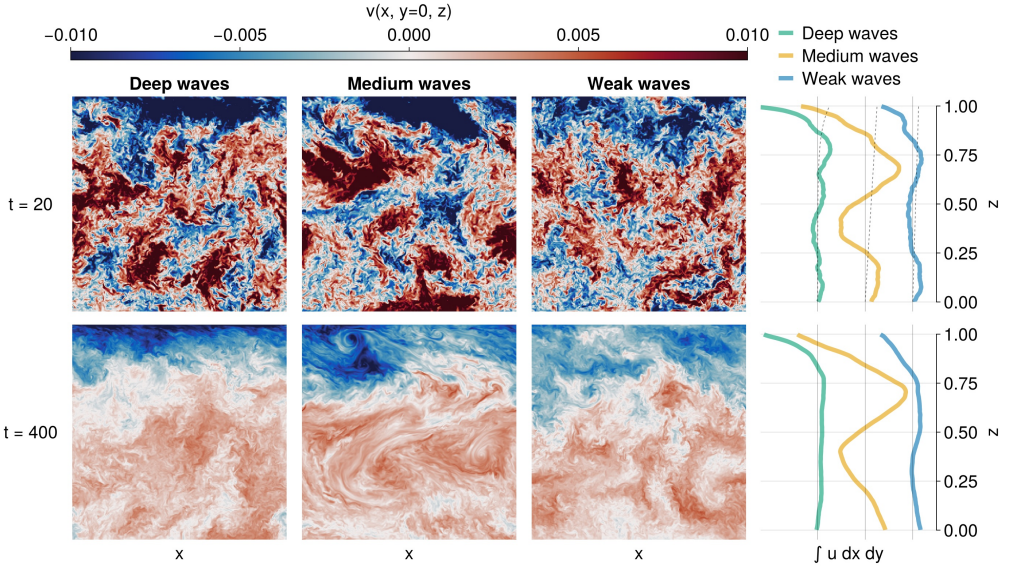

Figure 3: The evolution of cross-wave momentum v in the xz-plane (6 panels on the left) and horizontally-averaged along-wave-momentum u (2 panels on the right) at $t = 40, 400$ and for three wave fields: "deep" (left panel, red lines), "medium" (middle panel, orange lines), and "weak" (right panel, blue lines). Dashed lines in the top right plot show the Stokes drift profile (normalized) for each case. The u profiles and light gray "zero lines" are spaced apart by the scale $\delta u = 10^{-2}$. The u-profiles at right show the development of depth-alternating jets, including a counter-wave surface jet for all cases. The v-slices are similar between the three cases at early times, but at later times exhibit strong, localized wave-impacts in their respective regions of significant Stokes shear. Note that v plays the role that vertical velocity plays in rotating turbulence.

system

$$\frac{\mathrm{d}}{\mathrm{d}t}k = -\epsilon\,, \tag{3.2}$$

$$\frac{\mathrm{d}}{\mathrm{d}t}\epsilon = -a\frac{\epsilon^2}{k} - b\Omega\epsilon\,, \tag{3.3}$$

where $\epsilon(t)$ describes the dissipation rate of k, Ω is a characteristic scale for $\mathbf{\Omega}$, and a and b are $O(1)$ free parameters. Equation (3.2) follows from $\int \boldsymbol{u} \cdot (2.1)\,\mathrm{d}V$. The first term in (3.3) models the destruction of ϵ on the turbulent time-scale $\tau = k/\epsilon$, since $\mathrm{d}\epsilon/\mathrm{d}t \sim -\epsilon/\tau$ when $\Omega\epsilon \ll \epsilon/\tau$.

The second term in (4) models the suppression of kinetic energy dissipation — or alternatively, the growth of the correlation length due to the coalescence of coherent structures — by the background vorticity Ω. The relative importance of "intrinsic" destruction of ϵ and background-vorticity-induced destruction of ϵ is measured by the non-dimensional number $\Omega\tau = \Omega k/\epsilon$, whose significance is revisited in section 4. We note that (3.2) is exact — and unchanged whether or not the system is rotating or modulated by surface waves. The modulation of turbulence by surface waves is therefore fundamentally "catalytic", and can only affect k indirectly by changing (3.3).

The free parameter a may be constrained by considering isotropic turbulence with $\Omega = 0$. In this case we expect the turbulent kinetic energy to decay according to $k \sim t^{6/5}$ (Saffman

1967), which implies $\frac{\mathrm{d}}{\mathrm{d}t}k = -\frac{6}{5}\frac{k}{t}$, and thus in turn, via (3.2), leads to

$$\epsilon = -\frac{6}{5}\frac{k}{t}\,, \quad \text{so that} \quad \frac{\mathrm{d}}{\mathrm{d}t}\epsilon = -\frac{11}{5}\frac{k}{t^2}\,. \tag{3.4}$$

Inserting (3.4) into (3.3) yields $a = 11/6$.

The system (3.2)–(3.3) may be solved by forming $\epsilon^{-1}(3.3) - k^{-1}(3.2)$, which yields

$$\frac{\mathrm{d}}{\mathrm{d}t}\left(\log\epsilon - a\log k\right) = -b\Omega\,. \tag{3.5}$$

Integrating (3.5) produces

$$\log\frac{\epsilon}{\epsilon_0} = a\log\left(\frac{k}{k_0}\mathrm{e}^{-b\Omega t}\right)\,, \tag{3.6}$$

where ϵ_0 and k_0 are the dissipation and kinetic energy at $t = 0$. Inserting (3.6) into (3.2), integrating in time and rearranging then produces the solution

$$\frac{k}{k_0} = k_0\left\{1 + \frac{1}{nb\Omega}\frac{\epsilon_0}{k_0}\left(1 - \mathrm{e}^{-b\Omega t}\right)\right\}^{-n}\,, \tag{3.7}$$

where $n = 1/(a-1) = 6/5$. Taking the limit $\Omega \to 0$ (or $t \to 0$ with finite Ω), we obtain the corresponding solution for isotropic turbulence,

$$k_{\mathrm{isotropic}}(t) = k_0\left(1 + \frac{1}{n}\frac{\epsilon_0}{k_0}t\right)^{-n}\,, \tag{3.8}$$

which yields the expected power law $k \sim t^{-n}$ when $\epsilon_0 t/nk_0 \gg 1$.

At long times the isotropic and vortical solutions diverge: $k_{\mathrm{isotropic}} \to 0$ as $t \to \infty$, while in the vortical case k/k_∞ limits to the constant

$$\frac{k_\infty}{k_0} = \left(1 + \frac{\epsilon_0}{nb\Omega k_0}\right)^{-n}\,, \tag{3.9}$$

where $k_\infty = \lim_{t\to\infty} k(t)$. Equation (3.9) yields a formula for b in terms of k_∞,

$$b\Omega = \frac{\epsilon_0}{nk_0}\frac{1}{\left(\frac{k_\infty}{k_0}\right)^{1/n} - 1}\,, \tag{3.10}$$

which we use to diagnose b from our numerical simulations.

The dashed curves in figure 4 show solutions to the two-equation system in (3.2)–(3.3) that correspond to the solid-line simulated results. Figure 4 shows that a single value of $b = 0.036$ qualitatively describes the evolution of kinetic energy beneath surface waves for a wide range of background vorticity magnitudes Ω, where we estimate Ω with $\Omega \approx \int \partial_z u^{\mathrm{S}}\,\mathrm{d}z$. For the rotating case, we use $b = 0.033$ and $\Omega = 1/4$. While qualitatively excellent considering that $b \approx 0.036$ describes a wide range of conditions, we also find that the phenomenological model overestimates the dissipation rate — and therefore underestimates the kinetic energy k — during the transition between isotropic and background-vorticity-dominated regimes.

4. Discussion

In this paper we point out the similarity between rotating turbulence on the beta-plane and turbulence beneath surface waves. In particular, turbulence beneath surface waves exhibits the formation of coherent structures, the development of zonal jets, and the suppression of kinetic energy dissipation. These features are consistent with known properties of turbulence beneath surface waves, but the connection with rotating turbulence is obscured in the vast

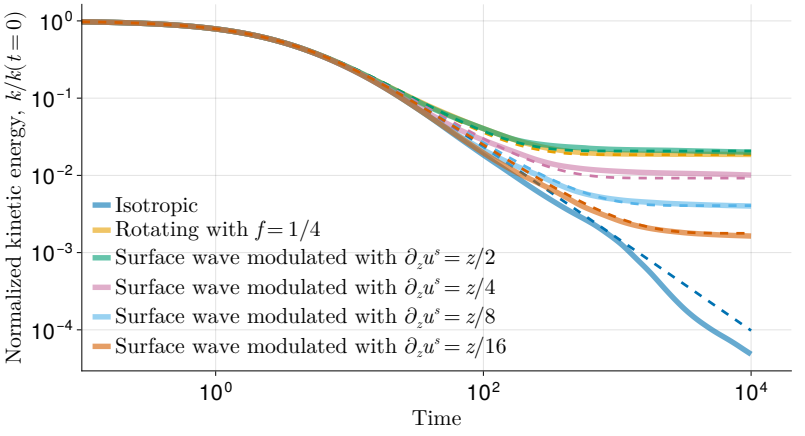

Figure 4: The decay of kinetic energy $k(t)$ in isotropic, rotating, and surface-wave-modulated turbulence. Solid lines show kinetic energy normalized by it's initial value, k/k_0, computed from large eddy simulations. Dashed lines show k/k_0 given by (3.7), which solves the phenomenological two-equation system in (3.2)–(3.3). The initial dissipation rate ϵ_0 in (3.7) is computed numerically from $k(t)$. We use $a = 11/6$ and estimate b from (3.10). For the rotating case, $\Omega = 1/4$ yields $b = 0.033$. For the four surface-wave-modulated cases we use $b = 0.036$, where $\Omega \overset{\text{def}}{=} \int \partial_z u^S \, \mathrm{d}z = (1/4, 1/8, 1/16, 1/32)$. Note that using $a = 1.75$ along with commensurate adjustments to b matches the simulation data even more closely.

majority of studies that also involve surface wind stress, ambient Lagrangian-mean shear, and surface forcing.

We exploit the connection to rotating turbulence by adapting a phenomenological two-equation model proposed by Bardina *et al.* (1985). In this two-equation model, the evolution of dissipation is affected by two terms: one "classical" term producing power-law decay of kinetic energy, and a second term that describes the suppression of kinetic energy dissipation by the presence of surface waves, which in turn effectively enhances kinetic energy levels and turbulent mixing relative to pure isotropic turbulence.

This phenomenological model hints at a new way to understand how surface waves enhance turbulent mixing. In the paradigm proposed by McWilliams *et al.* (1997), the effect of surface waves on turbulence is associated with the "Stokes contribution" to shear production in the turbulent kinetic energy budget. However, our results show that this interpretation must be incomplete, because surface waves also control the evolution of initially shear-free flows. We suggest that the impact of surface waves may be instead linked to their tendency to catalyze, without exchanging energy, an increase in the correlation times and length scales of turbulent motions. A benefit to this interpretation is that turbulent shear production can be interpreted in the standard way: as a transfer of kinetic energy from the horizontally-averaged, Lagrangian-mean velocity, whose energy is otherwise conserved. In other words, our descriptive analysis leads to an alternative paradigm for wave-modified turbulence wherein shear production is "unchanged" relative to wave-free turbulence (as in rotating turbulence). Instead of modifying shear production directly, then, waves impact both mixing and kinetic energy by inducing an inverse cascade, increasing the turbulent mixing length, and suppressing kinetic energy dissipation.

4.1. *The "pseudovorticity" number*

The analogy with rotating turbulence leads to a new non-dimensional number for characterizing surface wave effects on turbulence. In rotating turbulence, the Rossby number measures the relative magnitude of the relative vorticity $\boldsymbol{\nabla}\times\boldsymbol{u}$ and the background vorticity, $f\hat{\boldsymbol{z}}$, such that

$$\mathrm{Ro}\overset{\mathrm{def}}{=}\frac{|\boldsymbol{\nabla}\times\boldsymbol{u}|}{f}\sim\frac{U}{fL}\,, \tag{4.1}$$

where U is a characteristic horizontal velocity scale and L is a characteristic turbulent horizontal scale. We propose the analogous "pseudovorticity number" for boundary layer turbulence,

$$\mathrm{Ps}\overset{\mathrm{def}}{=}\frac{|\boldsymbol{\nabla}\times\boldsymbol{u}|}{|\partial_z\boldsymbol{u}^{\mathrm{S}}|}\sim\frac{W}{\Omega H}\,, \tag{4.2}$$

where W is a vertical velocity scale, Ω is the magnitude of the Stokes drift, and H is a vertical length scale. Ps measures the average role of surface waves with Stokes shear magnitude Ω on turbulent motions with vertical velocity scale W and turbulent scale H. In the two-equation model in (3.2)–(3.3), $\mathrm{Ps}\sim\epsilon/k\Omega$. In our decaying scenarios, Ps eventually vanishes at $t\to\infty$ and dissipation is completely suppressed.

4.2. *Connection with the Langmuir number*

The pseudovorticity number is connected between the Langmuir number — the usual non-dimensional quantity used to characterize the effect of waves on turbulence — when considering an estimate of Ps integrated over deep boundary layers. One definition of the Langmuir number is (McWilliams *et al.* 1997),

$$\mathrm{La}\overset{\mathrm{def}}{=}\sqrt{\frac{u_\star}{u^{\mathrm{S}}(z=0)}}\,, \tag{4.3}$$

where $u_\star\overset{\mathrm{def}}{=}\sqrt{\tau}$ is the friction velocity, which is the square root of the kinematic wind stress τ. At face value La does not apply to decaying cases, but we can amend this by interpreting $u_\star$ more generally as a turbulent velocity scale.

To connect La and Ps, we consider a "bulk" estimate of Ps over a wind-forced boundary layer of depth H, where the turbulent velocity scale is $W=u_\star$ and the turbulent length scale is H. If $u^{\mathrm{S}}(z=-H)$ is negligible, then estimating the pseudovorticity scale Ω as the average value over the boundary layer yields

$$\Omega\sim\frac{1}{H}\int_{-H}^{0}\partial_z u^{\mathrm{S}}\,\mathrm{d}z\sim\frac{u^{\mathrm{S}}(z=0)}{H}\,, \tag{4.4}$$

such that

$$\text{bulk Ps}=\frac{W}{\Omega H}\sim\frac{u_\star}{u^{\mathrm{S}}(z=0)}\sim\mathrm{La}^2\,. \tag{4.5}$$

We thus find that La^2 may be regarded as a bulk estimate of the more locally-applicable Ps, computed over the depth of the boundary layer, H. The difference between the bulk estimate La and the more specific estimate Ps resolves a paradox associated with La in that it depends on u^{S}, despite that only $\partial_z u^{\mathrm{S}}$ appears in (2.1).

Acknowledgements. Without implying their endorsement, we would like to acknowledge fruitful discussions with Bruno Deremble, Petros Ioannou, and Bill Young.

Funding. G.L.W. was supported by the National Science Foundation, grant OCE-2342715. N.C.C. was

supported by the Australian Research Council under DECRA Fellowship DE210100749, by the Center of Excellence for the Weather of the 21st Century CE230100012, and the Discovery Project DP240101274.

Declaration of interests. The authors report no conflict of interest.

Data availability statement. Scripts to reproduce the simulations and analyses in this of this study are openly available at GitHub repository github.com/glwagner/WaveAveragedDecayingTurbulence.

Author ORCIDs. Gregory L. Wagner, 0000-0001-5317-2445; Navid C. Constantinou, 0000-0002-8149-4094.

References

Bardina, J., Ferziger, J. H. & Rogallo, R. S. 1985 Effect of rotation on isotropic turbulence: computation and modelling. *Journal of Fluid Mechanics* **154**, 321–336.

Batchelor, G. K. 1953 *The theory of homogeneous turbulence*. Cambridge University Press.

Constantinou, N. C. 2015 Formation of large-scale structures by turbulence in rotating planets. PhD thesis, National and Kapodistrian University of Athens, Athens, Greece.

Constantinou, N. C., Farrell, B. F. & Ioannou, P. J. 2014 Emergence and equilibration of jets in beta-plane turbulence: Applications of Stochastic Structural Stability Theory. *Journal of the Atmospheric Sciences* **71** (5), 1818–1842.

Craik, A. D. D. & Leibovich, S. 1976 A rational model for Langmuir circulations. *Journal of Fluid Mechanics* **73** (3), 401–426.

Fan, Y., Yu, Z., Savelyev, I., Sullivan, P. P., Liang, J.-H., Haack, T., Terrill, E., de Paolo, T. & Shearman, K. 2020 The effect of Langmuir turbulence under complex real oceanic and meteorological forcing. *Ocean Modelling* **149**, 101601.

Farrell, B. F. & Ioannou, P. J. 2007 Structure and spacing of jets in barotropic turbulence. *Journal of the Atmospheric Sciences* **64** (10), 3652–3665.

Farrell, B. F. & Ioannou, P. J. 2019 *Statistical State Dynamics: A new perspective on turbulence in shear flow*, p. 380–400. Cambridge University Press.

Harcourt, Ramsey R 2015 An improved second-moment closure model of langmuir turbulence. *Journal of Physical Oceanography* **45** (1), 84–103.

Harcourt, R. R. & D'Asaro, E. A. 2008 Large-eddy simulation of Langmuir turbulence in pure wind seas. *Journal of Physical Oceanography* **38** (7), 1542–1562.

Holm, D. D. 1996 The ideal Craik-Leibovich equations. *Physica D: Nonlinear Phenomena* **98** (2-4), 415–441.

Huang, H.-P. & Robinson, W. A. 1998 Two-dimensional turbulence and persistent zonal jets in a global barotropic model. *Journal of the Atmospheric Sciences* **55** (4), 611–632.

Large, W. G., Patton, E. G., DuVivier, A. K., Sullivan, P. P. & Romero, L. 2019 Similarity theory in the surface layer of large-eddy simulations of the wind-, wave-, and buoyancy-forced southern ocean. *Journal of Physical Oceanography* **49** (8), 2165–2187.

Marston, J. B. & Tobias, S. M. 2023 Recent developments in theories of inhomogeneous and anisotropic turbulence. *Annual Review of Fluid Mechanics* **55**, 351–375.

McWilliams, J. C., Sullivan, P. P. & Moeng, C.-H. 1997 Langmuir turbulence in the ocean. *Journal of Fluid Mechanics* **334**, 1–30.

Polton, J. A., Lewis, D. M. & Belcher, S. E. 2005 The role of wave-induced Coriolis–Stokes forcing on the wind-driven mixed layer. *Journal of Physical Oceanography* **35** (4), 444–457.

Ramadhan, A., Wagner, G. L., Hill, C., Campin, J.-M., Churavy, V., Besard, T., Souza, A., Edelman, A., Ferrari, R. & Marshall, J. 2020 Oceananigans.jl: Fast and friendly geophysical fluid dynamics on GPUs. *Journal of Open Source Software* **5** (53), 2018.

Rhines, P. B. 1975 Waves and turbulence on a beta-plane. *Journal of Fluid Mechanics* **69** (3), 417–443.

Saffman, P. G. 1967 The large-scale structure of homogeneous turbulence. *Journal of Fluid Mechanics* **27** (3), 581–593.

Shu, C.-W. 2020 Essentially non-oscillatory and weighted essentially non-oscillatory schemes. *Acta Numerica* **29**, 701–762.

Srinivasan, K. & Young, W. R. 2012 Zonostrophic instability. *Journal of the Atmospheric Sciences* **69** (5), 1633–1656.

Sullivan, P. P. & McWilliams, J. C. 2010 Dynamics of winds and currents coupled to surface waves. *Annual Review of Fluid Mechanics* **42** (1), 19–42.

Suzuki, N. & Fox-Kemper, B. 2016 Understanding Stokes forces in the wave-averaged equations. *Journal of Geophysical Research: Oceans* **121** (5), 3579–3596.

Van Roekel, L. P., Fox-Kemper, B., Sullivan, P. P., Hamlington, P. E. & Haney, S. R. 2012 The form and orientation of Langmuir cells for misaligned winds and waves. *Journal of Geophysical Research: Oceans* **117** (C5).

Wagner, G. L., Chini, G. P., Ramadhan, A., Gallet, B. & Ferrari, R. 2021 Near-inertial waves and turbulence driven by the growth of swell. *Journal of Physical Oceanography* **51** (5), 1337–1351.

Wagner, G. L., Silvestri, S., Constantinou, N. C., Ramadhan, A., Campin, J.-M., Hill, C., Chor, T., Strong-Wright, J., Lee, X. K., Poulin, F., Souza, A., Burns, K. J., Marshall, J. & Ferrari, R. 2025 High-level, high-resolution ocean modeling at all scales with Oceananigans. *arXiv preprint* , arXiv: 2502.14148.